DOI:10.1158/0008-5472.CAN-03-2073

Cancer Research

Pseudopalisades in Glioblastoma Are Hypoxic, Express Extracellular Matrix Proteases, and Are Formed by an Actively Migrating Cell Population

Daniel J. Brat, Amilcar A. Castellano-Sanchez, Stephen B. Hunter, et al.

Cancer Res 2004;64:920-927. Published online February 10, 2004.

DOI:10.1158/0008-5472.CAN-03-2073

[CANCER RESEARCH 64, 920–927, February 1, 2004]

Pseudopalisades in Glioblastoma Are Hypoxic, Express Extracellular Matrix Proteases, and Are Formed by an Actively Migrating Cell Population

Daniel J. Brat,[1] Amilcar A. Castellano-Sanchez,[1] Stephen B. Hunter,[1] Marcia Pecot,[1] Cynthia Cohen,[1] Elizabeth H. Hammond,[3] Sarojini N. Devi,[2] Balveen Kaur,[2] and Erwin G. Van Meir[2]

Departments of [1]Pathology and Laboratory Medicine and [2]Neurosurgery and Hematology/Oncology and Winship Cancer Institute, Emory University School of Medicine, Atlanta, Georgia, and [3]Department of Pathology, LDS Hospital, Salt Lake City, Utah

ABSTRACT

Necrosis and vascular proliferation are the pathologic features that distinguish the most malignant infiltrative astrocytoma, glioblastoma (GBM), from those of lower grades. In GBM, hypercellular zones called pseudopalisades typically surround necrotic foci. Although these cells are known to secrete high levels of proangiogenic factors that promote tumor growth, their origins are ill defined. We propose that pseudopalisades represent differing stages and histologic samplings of astrocytoma cells migrating away from a hypoxic/anoxic focus, often triggered by a central vaso-occlusive event. This proposition is based on our findings that pseudopalisading cells are 5–50% less proliferative and 6–20 times more apoptotic than adjacent astrocytoma, indicating that cell accumulation does not result from increased proliferation or resistance to apoptosis. Coexisting inflammatory cells account for <2% of pseudopalisading cells and cannot account for hypercellularity. Pseudopalisading cells show nuclear expression of hypoxia-inducible factor 1α, consistent with their hypoxic nature, and hypoxia induces a 20–60% increase in glioma cell migration *in vitro*. Hypoxic cells *in vitro* and pseudopalisades in GBM specimens show enhanced gelatinase activity, typical of an invasive phenotype. These results suggest that pseudopalisading cells are migrating at the periphery of a hypoxic center. To uncover a potential source of hypoxia and sequence of structural events leading to pseudopalisade formation, we performed a morphometric analysis of 234 pseudopalisades from 85 pretreatment GBMs. We found distorted, degenerating, or thrombosed blood vessels within the center of more than half the pseudopalisades, suggesting that at least a subset of pseudopalisades are two-dimensional histologic representations of tumor cells migrating away from a vaso-occlusive event.

INTRODUCTION

Glioblastoma (GBM) is the most common and highest grade astrocytoma. The pathologic features that distinguish it from lower grade tumors are the presence of necrosis and a specialized form of angiogenesis, microvascular hyperplasia (1, 2). Necrotic foci in GBM are typically surrounded by hypercellular zones referred to as pseudopalisades (3, 4). The emergence of pseudopalisades and microvascular hyperplasia heralds the onset of aggressive growth, and these elements are thought to be mechanistically instrumental in malignant progression.

The intimate relationship between pseudopalisades and vascular proliferation in nearby regions is beginning to be understood (5, 6). Most studies indicate that pseudopalisading cells express high levels of vascular endothelial growth factor (VEGF) because of increased transcriptional activity of hypoxia-inducible factors 1 and 2 (HIF-1 and -2; Refs. 7–9). Secretion of VEGF, in turn, causes endothelial proliferation and angiogenesis, which takes the form of microvascular hyperplasia and glomeruloid bodies in GBM and other tumors (6, 10).

In contrast to our understanding of the angiogenic events that follow pseudopalisade formation, the pathogenesis of the pseudopalisading cells that initiate this sequence is not well defined (11–14). This hypercellular population potentially could represent (*a*) rapidly proliferating neoplastic cells that have "outgrown their blood supply" and undergone central necrosis; (*b*) a population resistant to apoptosis, which has accumulated because of increased cell survival; (*c*) a mixed population of tumor and inflammatory cells adjacent to necrosis; or (*d*) a population of cells migrating to or from a central focus.

We addressed the first three possibilities by studying pseudopalisades in human GBM specimens for proliferative activity, apoptotic rates, and potential inflammatory components. We addressed the fourth possibility by investigating whether hypoxia affected the migration of glioma cells or the expression of extracellular proteolytic enzymes associated with invasive properties, such as matrix metalloproteinases (MMPs) and the urokinase-dependent plasminogen-activating cascade. We also performed a morphometric analysis on a series of pseudopalisades in pretreatment GBM specimens to determine whether their features would be compatible with a sequence that included vaso-occlusion, hypoxia, increased tumor cell migration, and central necrosis.

MATERIALS AND METHODS

Immunohistochemistry. Archived surgically resected GBM specimens were retrieved from Emory University Hospital Department of Pathology. GBMs were selected from patients with no previous treatment with radiation or chemotherapy, and individual tissue blocks were chosen based on their content of pseudopalisades (from three to nine pseudopalisades per section). Tissues had been fixed previously in 10% buffered formalin, routinely processed, and embedded in paraffin. Immunohistochemical (IHC) studies were performed on 6-μm sections. Sections were deparaffinized and subjected to heat-induced epitope retrieval by steaming for 15 min. Slides then were incubated at room temperature with antibodies directed toward MIB-1 (mouse monoclonal, 1:160; Dako, Carpentaria, CA), caspase-3 (rabbit polyclonal, 1:25; Cell Signaling, Beverly, MA), cleaved caspase-3 (rabbit polyclonal, 1:100; Cell Signaling), CD68 (KP-1, mouse monoclonal, 1:2560; Dako), CD45 (LCA, mouse monoclonal, 1:1280; Dako), HIF-1α (mouse monoclonal, 1:5000; Novus-Biologicals, Littleton, CO), and urokinase-type plasminogen activator receptor (uPAR; mouse monoclonal, #3936, 1:200; American Diagnostica, Stamford, CT). Antibodies were detected using the avidin-biotin-peroxidase complex method using 3,3′-diaminobenzidine as the chromogen. Standard positive controls were used throughout. Normal sera served as the negative control. Sections were counterstained with hematoxylin.

Quantitation of Proliferation Indices, Apoptosis, and Inflammatory Cells. The percentage of cells showing nuclear staining for MIB-1 was quantitated independently by manual counting and by image cytometric analysis on separate tumor sets. For manual counts, the total number of tumor nuclei and those staining for MIB-1 were counted in three pseudopalisades for each of the nine GBMs by one of the authors (D. J. B.). Similar counts were made in the region of infiltrating astrocytoma directly adjacent to each pseudopalisade. Each count tallied a minimum of 250 cells. For cytometric analysis of MIB-1 proliferation, a CAS 200 image cytometer (Becton Dickinson Cellular Imaging

Received 7/11/03; revised 10/7/03; accepted 10/31/03.

Grant support: United States Public Health Service NIH Grants NS-42934 (D. J. Brat), CA-86335, CA-87830, and NS-41403 (E. G. Van Meir).

The costs of publication of this article were defrayed in part by the payment of page charges. This article must therefore be hereby marked *advertisement* in accordance with 18 U.S.C. Section 1734 solely to indicate this fact.

Requests for reprints: Daniel J. Brat, Department of Pathology and Laboratory Medicine, Emory University Hospital, H-176, 1364 Clifton Road NE, Atlanta, GA 30322. Phone: 404-712-1266; Fax: 404-727-3133; E-mail: dbrat@emory.edu; or Erwin G. Van Meir, Laboratory of Molecular Neuro-Oncology, Winship Cancer Institute, Emory University, 1365-C Clifton Road NE, Room C5078, Atlanta, GA 30322. Phone: 404-778-5563; Fax: 404-778-5240; E-mail: evanmei@emory.edu.

DOI:10.1158/0008-5472.CAN-03-2073

Systems, San Jose, CA) quantitated nuclear area that stained with 3,3′-diaminobenzidine (brown) compared with total nuclear area stained with hematoxylin (blue). At 620 nm, brown and blue nuclei absorb, giving a measure of total nuclear area. At 500 nm, only brown staining nuclei absorb, giving a measure of MIB-1 staining nuclei. For each of 10 GBMs (distinct from those used for manual counting), 15 fields were captured in regions of pseudopalisading cells and adjacent infiltrative astrocytoma.

For assessing apoptosis, the number of cleaved caspase-3-expressing cells and total cells were counted in three pseudopalisades and regions of adjacent astrocytoma from nine GBM specimens (15). In these same specimens, the percentage of LCA-positive lymphocytes and CD68-positive macrophages in pseudopalisades and adjacent astrocytoma was calculated. For studies of proliferation, apoptosis, and inflammatory infiltrates, mean and SE were calculated for pseudopalisades and adjacent astrocytoma. A two-sided Student's *t* test was performed for significance ($P < 0.05$).

Glioblastoma Cell Lines and Culture Conditions. Human glioblastoma cell lines (LN229, 2024, and WT11) and their cell culture conditions have been described previously (16). Cells were grown to 80% confluence in 100-mm culture dishes, placed in serum-free media at 37°C in incubators in conditions of 20% O_2 (normoxia), 1% O_2 (hypoxia), or in 300 μM $CoCl_2$. For experiments in 1% O_2, culture dishes were placed in small Modular Incubator Chambers (Billups-Rothenberg, Del Mar, CA), which were flushed with 94% N_2, 5% CO_2, and 1% O_2, and then stored in 37°C incubators. After 24 h, cell pellets and conditioned media were collected and immediately frozen at −70°C. For protein analysis, cells were lysed immediately before use in 50 mM Tris-Cl (pH 6.8), 100 mM DTT, 2% SDS, 0.1% bromphenol blue, and 10% glycerol.

***In Vitro* Cell Migration.** A total of 5×10^4 LN229, WT11, or 2024 cells were plated into the upper compartment of modified Boyden chambers (BD Biocoat, Becton Dickinson Labware, Bedford, MA) in 24-well plates. Top compartments contained 0.5 ml DMEM/10% fetal bovine serum, and bottom compartments contained 0.75 ml of DMEM/10% fetal bovine serum. Chamber inserts separating the upper and lower compartments contained 8-μm pores and were uncoated. Cells were allowed to migrate for 4, 8, 16, or 24 h at 37°C in 20% O_2 or 1% O_2. Cells remaining on the top of the insert were removed by wiping with cotton swabs. Migrated cells on the bottom of the insert were fixed in methanol and stained with a Diff-Quik Stain Set (Dade Behring, Newark, DE). Total cells were counted using a stage micrometer within a central 6.25-mm^2 grid, which accounted for 14% of the surface area of the insert. Experiments were performed in triplicate, with the resulting mean and SE from hypoxic and normoxic conditions being compared by a two-sided Student's *t* test for significance ($P < 0.05$).

Western Blot Analysis. Immunoblots were performed on protein from cell lysates from indicated cell lines. Equal amounts of protein (30 μg) were resolved on a 10% SDS-PAGE and transferred to nitrocellulose membranes. Blots were probed with mouse monoclonal anti-HIF-1α antibody (1:750; BD Biosciences, Franklin Lakes, NJ) or mouse monoclonal uPAR (1:250; #3937, American Diagnostica), incubated with horseradish peroxidase conjugated to goat antimouse antibody (1:1000; Dako), and developed by enhanced chemiluminescence reagents (Pierce Biotechnology, Rockford, IL). Actin blots were developed by goat antihuman actin antibody (1:500, Santa Cruz Biotechnology Inc., Santa Cruz, CA), followed by horseradish peroxidase-conjugated swine antigoat antibody (1:1000; Roche Molecular Biochemicals, Indianapolis, IN), and visualized by enhanced chemiluminescence.

Gel Zymography. Gelatinolytic activity of serum-free conditioned media was assessed by gelatin zymography for LN229 cells grown for 24 h in 20% oxygen, 1% oxygen, and 300 μM $CoCl_2$. Five hundred μl of conditioned media from each condition were concentrated fivefold using Centricon centrifugal filter devices (Millipore, Bedford, MA), and 60 μl were used for loading {loaded under nonreducing conditions with 10 μl electrophoresis buffer [350 mM Tris-HCl (pH 6.8), 10% SDS, 30% glycerol, and 0.1% bromphenol blue]}. Proteins were separated electrophoretically at 4°C in an 8% SDS-polyacrylamide gel containing 0.1% type B gelatin (Sigma Chemical Co., St. Louis, MO). The gel was rinsed three times for 20 min in 2.5% Triton X-100, followed by digestion [50 mM Tris-HCl (pH 7.5), 200 mm NaCl, 5 mM $CaCl_2$, and 0.02% NaN_3] at 37°C for 36 h. The gel then was stained with 0.05% Coomassie Blue in methanol, acetic acid, and H_2O (3:1:6) at room temperature for 1 h and destained in the same solution without Coomassie Blue three times for 15 min.

Activity of plasminogen activators was assessed in serum-free conditioned media from LN229 cells grown for 24 h in 20% O_2, 1% O_2, and 300 μM $CoCl_2$ by similar methods. Proteins were separated electrophoretically at 4°C in an 8% SDS-polyacrylamide gel containing 2 mg/ml α-casein and 0.025 units/ml of plasminogen (Sigma). Gels were rinsed, digested, stained, and destained as described previously.

***In Situ* Gel Zymography.** A thin film of 8% polyacrylamide gel containing 1% gelatin (no SDS) was allowed to dry onto charged histologic glass slides in a reduced oxygen environment (1% O_2 for 2 h). Frozen glioblastoma tissue sections (6 μm) on histologic slides then were applied to the gel, with the gel and tissue section directly contacting each other between a sandwich of glass slides. Gel and tissue were incubated together at 37°C for 6 h in digestion buffer (see above), after which the tissue section was removed. The gel was stained in 0.05% Coomassie Blue and destained as described previously. Regions on the gel corresponding to pseudopalisades on adjacent H&E-stained sections were evaluated for gelatinase activity.

ELISA for Urokinase-Type Plasminogen Activator. Concentrations of uPA were determined by ELISA per the manufacturer's instructions (Imunobind uPA ELISA kit; American Diagnostica) on conditioned serum-free media obtained from LN229 cells exposed to 20% O_2, 1% O_2, or 300 μM $CoCl_2$ for 24 h.

Morphometric Analysis of Pseudopalisades. Morphometric analysis was performed by one of the authors (D. J. B.) on pseudopalisades within GBM specimens from the Radiation Therapy Oncology Group (RTOG) tissue repository from clinical trials RTOG 02–11, 00–23, 00–21, 98–06, 96–02, 93–05, and 90–06. The trials were chosen because enrolled patients had new-onset GBM (no recurrent neoplasms), substantial tissue resections rather than stereotactic biopsy, and no previous radiation therapy or chemotherapy. Patients fulfilled specific hematologic and laboratory criteria for clinical trial enrollment and therefore were unlikely to have blood-clotting disorders (for more information, see www.rtog.org).

Representative slides sent to the RTOG tissue bank were reviewed for the presence of pseudopalisades. Only pseudopalisades with a complete circumference within the tissue were analyzed. One hundred eighty-four tumors were reviewed, and 85 contained complete pseudopalisades that could be analyzed. Each of the 85 contained 1–12 pseudopalisades (average, 3 per tumor), yielding 234 pseudopalisades to be evaluated. The average cell density of pseudopalisading cells compared with adjacent astrocytoma was determined using a stage micrometer on 12 random pseudopalisades from six GBM specimens (Fig. 1). The areas studied in each instance measured 0.033 mm × 0.167 mm. Maximal internal width and lengths of each pseudopalisade were measured (Fig. 1). The presence of any vascular lumen within the internal circumference of the pseudopalisade was noted, as was the presence of thrombosis within the blood vessel. Thrombosis was defined as a solid deposition of platelets and fibrin that filled the entire vascular lumen. The internal content of the pseudopalisade was classified as either fibrillar or necrotic, and the presence of nuclear fragmentation and neuropil vacuolization was noted. If present, the distance from a central blood vessel to the nearest internal edge of

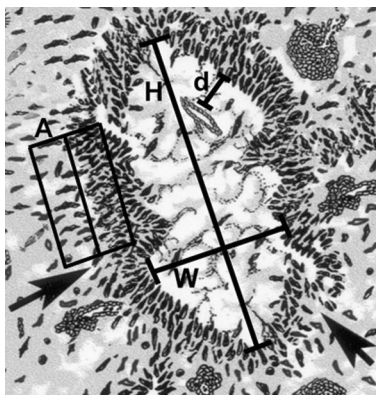

Fig. 1. Schematic representation of a pseudopalisade (*arrows*) indicating measurements made for the morphometric analysis. W = greatest internal width, H = greatest internal height (length), d = shortest distance from internal vessel (if present) to the internal pseudopalisade wall, and A = area analyzed for cell density in astrocytoma adjacent to pseudopalisade. Contents of pseudopalisade were characterized as fibrillar, vacuolated (degenerating), or necrotic.

DOI:10.1158/0008-5472.CAN-03-2073

the pseudopalisade was measured. Using a significance threshold of $P < 0.05$, χ^2 tests were performed to compare proportions of large (>200 μm) and small (<200 μm) pseudopalisades that had a given feature.

RESULTS

Cell Density Is Two Times Higher in Pseudopalisades than Adjacent Astrocytoma. To document the degree of increased cellular accumulation in pseudopalisades, we measured cell density in 12 pseudopalisades and adjacent astrocytoma from six GBM specimens (see box in Fig. 1*A* for example of areas counted). We found that the cell density (mean ± SE) in pseudopalisades was $1.95 \pm 0.16 \times 10^4$ cells/mm^2 as compared with $1.02 \pm 0.07 \times 10^4$ cells/mm^2 in adjacent astrocytoma ($P < 0.05$).

Pseudopalisades Are Less Proliferative than Adjacent Astrocytoma. Given the twofold increased cellularity of pseudopalisades, we measured proliferation rates to determine whether increased cell division accounted for cellular accumulation. MIB-1 is an antibody that recognizes the nuclear antigen Ki67, which is expressed in actively cycling cells but is absent from resting (G0) cells (17). MIB-1 proliferation indices were lower in pseudopalisades of GBMs than in adjacent astrocytoma for each GBM investigated as quantitated by two independent methods (Fig. 2). In the nine GBMs analyzed by manual counting, MIB-1 indices varied substantially in both pseudopalisades (range, 10–38%) and in adjacent astrocytoma (range, 20–41%). The percentage of neoplastic cells staining in pseudopalisades was lower than in the astrocytoma immediately next to it for each of the GBMs (average ± SE, 20.8 ± 2.8 in pseudopalisades *versus* 27.6 ± 3.0 in adjacent astrocytoma; $P < 0.05$; Fig. 2*B*).

In 10 separate GBMs, MIB-1 proliferation indices were quantitated by image cytometry, which measures the area of MIB-1 stained nuclei as a percentage of total nuclear area in a given field. MIB-1 proliferation indices varied from 5.0–12.5% in pseudopalisades and from 8.3–16.9% in adjacent astrocytoma. The MIB-1 proliferation index again was lower in pseudopalisades than in adjacent astrocytoma for each GBM (average ± SE, 7.9 ± 1.0 in pseudopalisades *versus* 12.4 ± 0.9 in adjacent tumor; $P < 0.05$; Fig. 2*C*). MIB-1 indices determined by image cytometry are typically lower than those determined by manual counting because the threshold for detecting nuclear MIB-1 by image cytometry is higher than visual detection (17). Lower proliferation indices in pseudopalisades indicated that their increased cellularity is not caused by increased proliferation.

Pseudopalisades Have Higher Rates of Apoptosis than Adjacent Astrocytoma. We next considered whether resistance to apoptosis could account for the hypercellularity of pseudopalisades by using an antibody that recognizes the cleaved, activated form of caspase-3, which is specific for cells undergoing apoptosis (15). IHC for cleaved (activated) caspase-3 in nine GBMs showed that the percentage of immunoreactive tumor cells was significantly higher in pseudopalisades than in adjacent astrocytoma (Fig. 3). The percentage of cells staining with cleaved caspase-3 varied from 0.3–2.1% within given pseudopalisades and from 0.02–0.2% within regions of adjacent astrocytoma. In each of the nine GBMs, the percentage of cleaved caspase-3 staining tumor cells was higher in pseudopalisades than adjacent astrocytoma, ranging from 6–20-fold greater (mean ± SE, 12.2- ± 1.4-fold; $P < 0.05$; Fig. 3*B*). IHC for (total) caspase-3 showed mild immunoreactivity of equal intensity in nearly all of the cells of pseudopalisades and adjacent astrocytoma. Because the antibody for caspase-3 also recognizes the cleaved protein fragment, occasional cells with more intense immunoreactivity were noted in the same distribution of cells that stained for cleaved caspase-3 (not shown). Thus, resistance to apoptosis did not cause cellular accumulation in pseudopalisades.

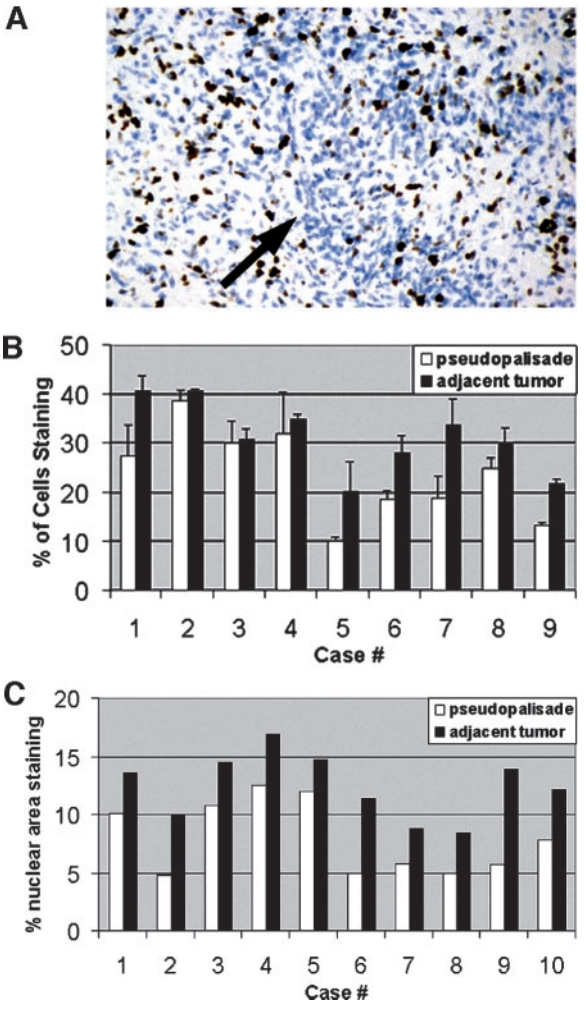

Fig. 2. Quantitation of proliferation rates in pseudopalisades. *A*, immunohistochemistry for MIB-1 on human glioblastoma specimen shows a lower percentage of nuclear staining in pseudopalisading cells (*arrow*) than in surrounding astrocytoma cells. *B*, MIB-1 proliferation indices were quantitated as percentage of cells staining by manual counting on nine cases. Error bars indicate SE for individual tumors. *C*, image cytometry was used to quantitate the percentage of nuclear area staining on 10 separate GBMs. In all of the tumors, proliferation rates were lower in pseudopalisading regions than in adjacent astrocytoma.

Pseudopalisades Do Not Contain a Prominent Inflammatory Component. Increased cellularity around necrosis could be because of an inflammatory infiltrate, so we investigated the presence of CD68-staining macrophages and CD45 (LCA)-staining lymphocytes in nine GBMs. CD68-positive macrophages were seen predominantly in a perivascular distribution and within the infiltrative component of astrocytomas immediately surrounding blood vessels. They accounted for <2% of total cells in pseudopalisading and infiltrative components (range, 0–2%). CD45-positive lymphocytes were even less common, accounting for <1% of total cells within the GBMs (range, 0–1%). The overall low numbers of macrophages and lymphocytes indicated that they do not account for the increased cellularity of pseudopalisades (not shown).

Pseudopalisading Cells and Hypoxic GBM Cells *in Vitro* Express HIF-1α. Results from the aforementioned studies left the possibility that pseudopalisades represent an actively migrating population, and we hypothesized cell migration might be related to hypoxia. IHC for HIF-1α performed on nine GBM specimens demonstrated strong nuclear staining in 20–30% of pseudopalisading cells, with little or no staining in adjacent tumor cells (Fig. 4, *A* and *B*). As a control for antibody specificity on formalin-fixed tissue and to dem-

DOI:10.1158/0008-5472.CAN-03-2073

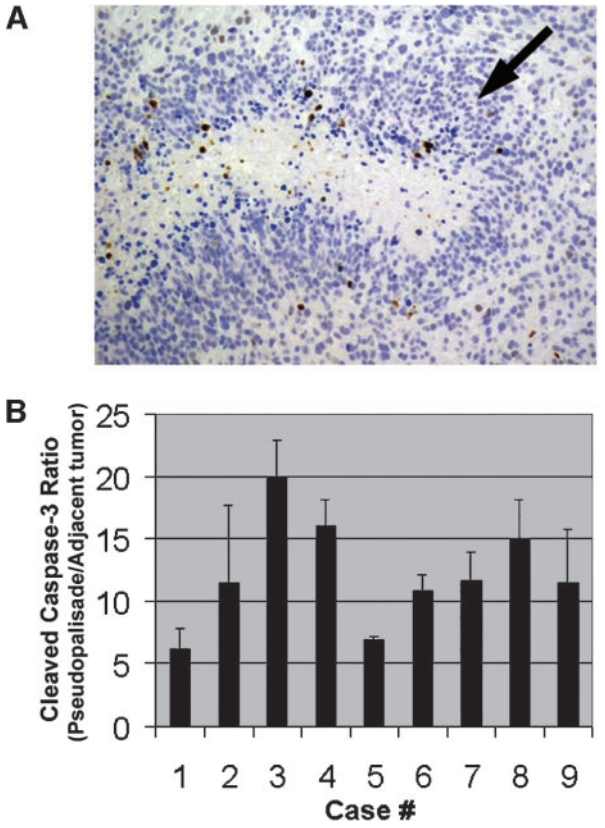

Fig. 3. Quantitation of apoptotic cells in pseudopalisades. *A*, immunohistochemistry for cleaved (activated) caspase-3 on human glioblastoma specimen demonstrated increased staining in the region of pseudopalisading as compared with adjacent astrocytoma. *B*, cells staining for activated caspase-3 were more numerous in pseudopalisades, with the ratio of staining in pseudopalisades to adjacent astrocytoma varying from 6–20. Error bars indicate SE for nine individual GBMs.

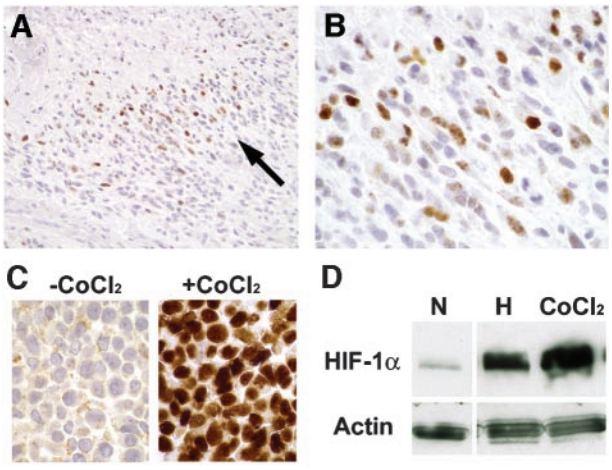

Fig. 4. Pseudopalisading and hypoxic glioma cells express hypoxia-inducible factor (*HIF*). *A* and *B*, low and high magnification of immunohistochemistry for HIF-1α performed on a human glioblastoma (GBM) demonstrating increased nuclear staining in pseudopalisades (*A*, *arrow*) but not adjacent astrocytoma. *C*, as a control for HIF-1α antibody specificity, immunohistochemistry of formalin-fixed LN229 GBM cells showed increased expression of HIF-1α only within the nucleus of cells exposed to 300 μM $CoCl_2$ for 24 h. *D*, Western blot analysis of cell lysates from 2024 GBM cells demonstrating increased HIF-1α expression in hypoxia (*H*; 1% O_2) and $CoCl_2$ (300 μm) compared with normoxia (*N*; 20% O_2).

onstrate similar hypoxic up-regulation of HIF-1α in our *in vitro* experiments, we performed IHC for HIF-1α on formalin-fixed LN229 cells grown in normoxia, $CoCl_2$ (Fig. 4*C*), or 1% O_2 (hypoxia, not shown) for 24 h. Increased expression of HIF-1α, specifically in the nucleus, was seen in cells exposed to hypoxia or $CoCl_2$ but was not noted in normoxic cells (Fig. 4*C*). Western blot analysis using cell lysates from 2024 (Fig. 4*D*) and LN229 (not shown) human GBM cells confirmed that hypoxia and $CoCl_2$ cause dramatic increases in HIF-1α protein expression.

Hypoxic GBM Cells Show Enhanced Migration *in Vitro*. We next tested whether hypoxic glioma cells *in vitro* were more migratory. Cell migration of 2024, WT11, and LN-229 cells after 24 h in modified Boyden chambers under normoxic conditions varied from 153 cells/mm^2 (2024) to 194 cells/mm^2 (WT11) to 430 cells/mm^2 (LN-229; Fig. 5, *A* and *C*). For all three cell lines, increased migration was seen under hypoxic conditions at 24 h (Fig. 5, *B* and *C*; $P < 0.05$ for each cell line). Migration increased most in hypoxia for 2024 cells compared with normoxia (60% increase). The 2024 cells that migrated under hypoxia also had morphologic differences from migrated normoxic cells. The former were more highly spindled, had larger cytoplasmic surface area, and more numerous cellular processes (Fig. 5*B*), whereas the latter were rounder or polygonal (Fig. 5*A*).

Hypoxic GBM cells and Pseudopalisades Show Enhanced Gelatinase Activity. Given the increased cellular migration noted in hypoxia, we next investigated whether extracellular matrix proteases associated with invasion, such as MMP-2 and -9, were expressed preferentially in hypoxic glioma cells. To examine whether gelatinase activity associated with MMP-2 or -9 expression might be present in pseudopalisades, we performed *in situ* gelatin zymography on frozen tissue sections of three human GBM specimens. All three demonstrated focal intense gelatinase activity in regions corresponding to pseudopalisades on H&E sections. These regions were seen as clear zones within the gelatin film directly overlying the pseudopalisades

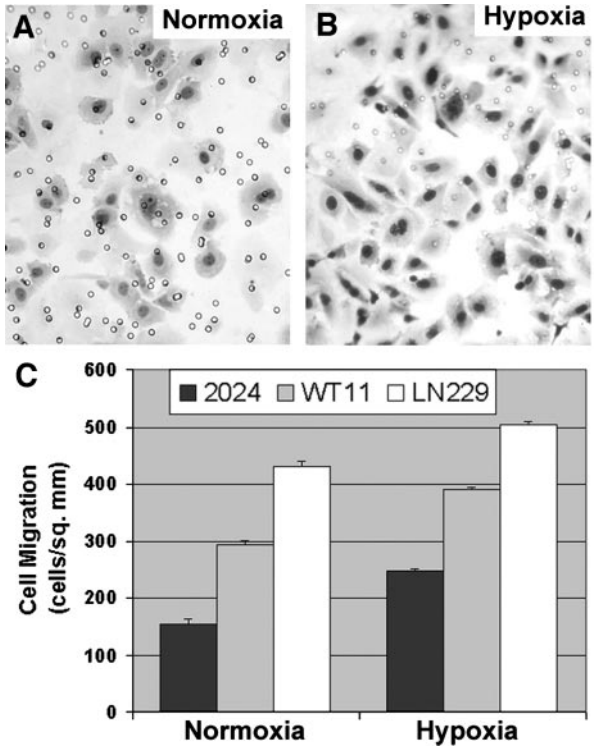

Fig. 5. Increased glioma cell migration under hypoxia. Photomicrograph of 2024 glioma cells after migration through 8-μm pores in a modified Boyden chamber under normoxia (*A*, 20% O_2) or hypoxia (*B*, 1% O_2). Pores can be seen in the background. *B*, more hypoxic cells have migrated through the membrane after 24 h, and individual hypoxic cells are more elongated, have larger surface areas, and have more extended cellular processes. *C*, quantitation by manual counting revealed that 2024, WT11, and LN229 glioma cells showed a 20–60% increase in cellular migration in hypoxia compared with normoxia after 24 h. Experiments were performed in triplicate. Error bars indicate SE.

DOI:10.1158/0008-5472.CAN-03-2073

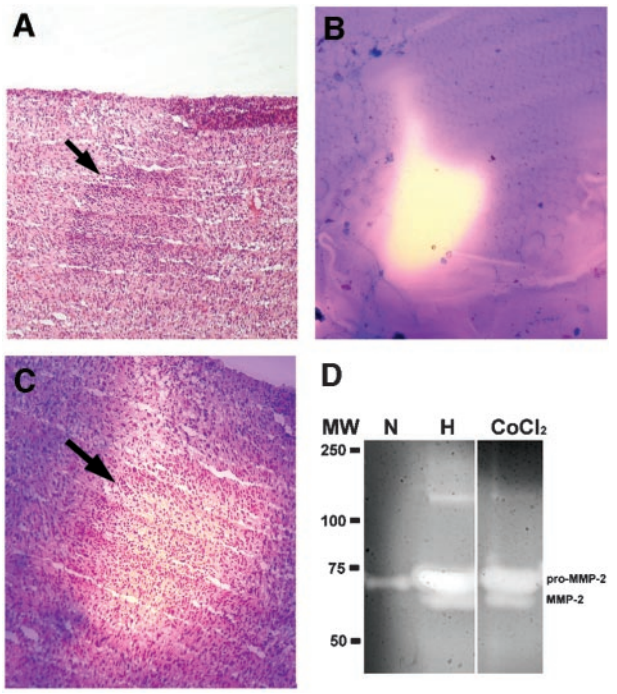

Fig. 6. Increased gelatinase activity in pseudopalisades and hypoxic glioma cells. *A*, H&E-stained frozen section of a human glioblastoma showing a single small pseudopalisade (*arrow*). *B*, *in situ* gelatin zymogram demonstrates gelatinase activity on an adjacent tissue section in the region of the pseudopalisade. *C*, overlay of the H&E-stained section and the gelatin zymogram showing the localization of the gelatinase activity to pseudopalisading cells. *D*, gelatin zymography performed on conditioned media collected from LN229 cells exposed for 24 h to normoxia (*N*; 20% O_2), hypoxia (*H*; 1% O_2), or 300 μM $CoCl_2$. The major gelatinolytic band at M_r 72,000 corresponds to pro-matrix metalloproteinase (*MMP*)-2, and the minor band at slightly lower molecular weight corresponds to activated MMP-2. MMP-2 gelatinase activity is markedly higher in conditioned media from hypoxia and $CoCl_2$ conditions than from normoxia. No MMP-9 band was noted (M_r 92,000).

(Fig. 6, *A–C*). Areas of gelatinase activity were slightly larger than pseudopalisades, suggesting that either the pseudopalisade in the section applied to the gel was larger than the adjacent H&E slide or the gelatinase activity extends slightly beyond the area of pseudopalisading. Adjacent regions corresponding to infiltrating astrocytoma showed patchy gelatinase activity but not the intense focal activity of pseudopalisades (not shown).

Gelatin zymography of conditioned media from LN229 cells demonstrated an increase in MMP-2 gelatinolytic bands from hypoxia and $CoCl_2$ exposed cells (Fig. 6*D*). Bands corresponding to pro-MMP-2 (M_r 72,000) and active MMP-2 (M_r 68,000) were markedly larger under these conditions. A minor band at M_r 140,000 also was noted in hypoxia and $CoCl_2$, likely representing an MMP-2 dimer. A gelatinolytic band at M_r 92,000 corresponding to MMP-9 was not detected under these conditions.

Hypoxic and Normoxic GBM Cells Express uPAR and Secrete uPA. The plasminogen-activating cascade, including secreted uPA and its cell surface receptor uPAR, are believed to be important for cellular migration and invasive behavior. ELISA analysis of uPA (urokinase) levels in conditioned media from LN229 cells exposed to normoxia showed a concentration of 1.9 $\pm$ 0.1 ng/ml, and levels were increased only modestly by hypoxia (2.1 $\pm$ 0.1 ng/ml). Likewise, gel zymography on the same media showed little difference in plasminogen activation between hypoxic and normoxic cells (not shown). Immunohistochemistry for the uPAR on GBM specimens showed roughly similar expression in pseudopalisades and adjacent astrocytoma, but uPAR expression was higher in neoplastic tissue than in non-neoplastic brain (not shown). Western blot analyses showed similar uPAR expression in normoxic and hypoxic LN229 cells (not shown).

Morphologic Features of Pseudopalisades Vary with Width. The aforementioned findings suggested that pseudopalisades represent a cell population migrating from hypoxia. We then wanted to uncover a sequence of structural events and potential sources of hypoxia/necrosis associated with pseudopalisade formation. We performed a morphometric analysis of pseudopalisades in a series of 184 cases of pretreatment GBMs (see "Materials and Methods"). We identified 85 that contained 234 complete pseudopalisades, ranging from 30 to 1500 μm in greatest internal width and from 50 to 3500 μm in greatest internal length (Fig. 1 and Table 1). We found that more than half of the pseudopalisades examined (55%) had evidence of a central vascular lumen, either viable (Fig. 7, *C* and *D*), degenerating (Fig. 7*E*), or thrombosed (Fig. 7*F*). Twenty percent of pseudopalisades contained a vessel with intravascular thrombosis, as evidenced by complete occlusion of the lumen by unorganized platelet and fibrin clot (Fig. 7*F*). We found that the percentage of pseudopalisades with internal vessel(s) or intravascular thrombus was related to the width of the pseudopalisade, with wide pseudopalisades (>200 μm) more frequently containing these elements than narrow ones (<200 μm; χ^2 test; $P < 0.05$; Table 1). All of the pseudopalisades >500 μm wide (Fig. 7*C*) had internal vessels, and 44% contained intravascular thrombosis. The presence of necrosis or central fibrillarity within pseudopalisades also correlated best with internal width: pseudopalisades with small widths, especially <100 μm, most often had fibrillar, non-necrotic centers (Fig. 7*A*). All of the pseudopalisades >500 μm had necrotic centers (Fig. 7*C*). Pseudopalisades characterized by a narrow (<100 μm) but long (>500 μm) shape (*i.e.*, serpiginous) were more likely to have fibrillar centers. In general, the distance from the vascular wall, when present, to the internal wall of the pseudopalisade increased with pseudopalisade width (Fig. 1 and Table 1). In the largest pseudopalisades, this distance averaged 33 μm (SD, 40 μm).

Because intravascular thrombosis was identified in a substantial subset of pseudopalisades and could represent potentially a central mechanism in their formation, we were interested in determining the overall frequency of intravascular thrombosis within entire GBM specimens. In a review of 103 random GBMs from our set of 184 cases, we identified microscopic intravascular thrombus within neoplastic tissue (either within pseudopalisades or adjacent astrocytoma) in 97 tumors (94%).

Table 1 *Relationship of pseudopalisade width to morphologic features*

Feature	Pseudopalisade width (μm)			
	<100 μm (n = 50)	100–200 μm (n = 69)	201–500 μm (n = 74)	>500 μm (n = 41)
Central vessel(s)	28%	38%	65%	100%
Central thrombosed vessel(s)	6%	9%	27%	44%
Fibrillar (non-necrotic) center	77%	59%	26%	0%
Necrotic center	23%	41%	74%	100%
Mean (SD) minimal vessel–Psp wall distance[a]	13.5 μm (8.7)	12.2 μm (14.5)	29.2 μm (32.8)	32.8 μm (39.8)

[a] Represents the distance from the outer vessel wall to the nearest internal side wall of the pseudopalisade (Psp).

DOI:10.1158/0008-5472.CAN-03-2073

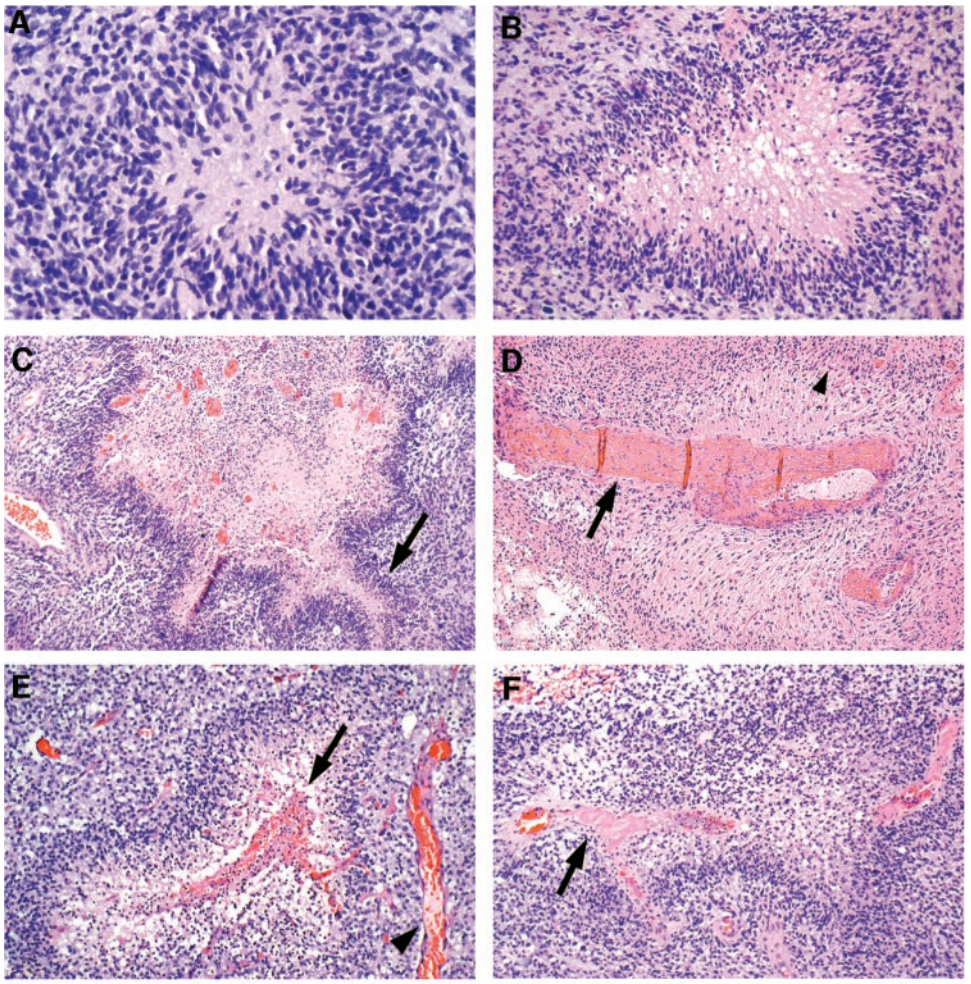

Fig. 7. Histopathologic features of pseudopalisades in glioblastoma (GBM). *A*, narrow pseudopalisades, especially those <100 μm wide, have hypercellular zones surrounding internal fibrillarity but usually lack central necrosis. *B*, medium-sized pseudopalisades (200–400 μm) are characterized by central necrosis, central vacuolization, and individual dying cells but typically have a peripheral zone of fibrillarity immediately inside the pseudopalisade. Note the absence of central vessels or vascular thrombosis in *A* and *B*. *C*, the largest pseudopalisades (those >500 μm) have extensive necrotic zones and nearly always have central vessels. Note the distance of vessels to the inner aspect of the pseudopalisade and the numerous outpouchings of pseudopalisades (*C*, *arrow*), which on tangential sectioning could give rise to smaller pseudopalisades resembling *A* or *B*. *D*, GBM cells "caught in the act" of forming a pseudopalisade (*arrowhead*) appear to be migrating away from an enlarged, distorted, and presumably dysfunctional vessel (*arrow*). Note the perivascular fibrillarity, lack of central necrosis, and streaming of tumor cells along fibrillar processes in this instance. *E*, in other cases, tumor cells appear to be migrating away from centrally degenerating vessels (*arrow*) and toward alternative vascular supplies (*arrowhead*). *F*, intravascular thrombosis (*arrow*) within a pseudopalisade (*F*). In *E* and *F*, pseudopalisading cells outline the shape of the internal vessel, suggesting outward migration.

DISCUSSION

Pseudopalisades are dense cellular arrangements that surround necrotic foci in GBM. Although their origin is unclear, they are pathognomonic of the disease. Understanding the mechanisms underlying their formation is of central importance because they are believed to contribute directly to the malignant behavior of GBMs. Pseudopalisading cells show increased HIF expression, resulting in high mRNA levels of the HIF target gene *vegf*. This sequence results in an exuberant angiogenic response that fuels neoplastic progression (5, 18–21).

Our studies show that cells in pseudopalisades have a lower proliferation index than adjacent cells. This finding does not support previous contentions that pseudopalisades represent a rapidly dividing tumor population that has "outgrown its blood supply" and undergone central necrosis (11, 12). The increased cellularity could not be explained by a decreased rate of apoptosis either, since pseudopalisading cells show higher rates of cleaved caspase-3 than adjacent cells (13–15). The twofold increased cell density could not be accounted for by a coexisting inflammatory component around the region of necrosis because inflammatory cells accounted for less than 2% of total cells in GBM. Among the possibilities considered, we hypothesized that pseudopalisades represent a population of neoplastic cells migrating from a central focus. The addition of outwardly migrating cells to a less motile population would result in the hypercellular zones seen in tissue sections. To validate this hypothesis, we needed to identify the cause of cell migration and the sequence of events leading to the pseudopalisading phenotype.

A salient physiologic feature that distinguishes pseudopalisading from surrounding cells is hypoxia (19–21). We confirmed that pseudopalisading cells express high nuclear levels of HIF-1α. HIF mediates an adaptive transcriptional response to hypoxia, which includes activation of glycolytic metabolism, secretion of proangiogenic factors, and increased cell migration (22, 23). In light of this, we examined whether pseudopalisading cells might be migrating from a central hypoxic region. Direct measures of cell migration cannot readily be performed in pathologic specimens. Therefore, we examined whether GBM cells in culture were more migratory under hypoxic conditions. We found that hypoxia induced a modest but reproducible (20–60%) increase in cell migration after 24 h depending on the cell line. This degree of enhanced migration could account easily for the twofold increase in cell density noted in pseudopalisades, which most likely form over the course of days to weeks. Our findings in gliomas agree with previous studies that have shown that hypoxia induces invasive behavior and a migratory phenotype in other forms of cancer, mostly by mechanisms that involve HIF-mediated transcription (23, 24). Moreover, the pharmacologic agent geldanamycin has been shown to inhibit HIF activity and reduce basal (normoxic) migration by glioma cells (25).

Hypoxic induction of cellular migration and invasion depends in part on HIF-mediated transcription of extracellular matrix proteases. Among the gene targets of HIF-1, MMP-2 (23, 26) and uPAR (27), the receptor for urokinase, are relevant to invasive behavior. MMP-2 and -9 (also referred to as gelatinase A and B, respectively) are expressed and secreted by malignant gliomas *in vivo* and can modu-

DOI:10.1158/0008-5472.CAN-03-2073

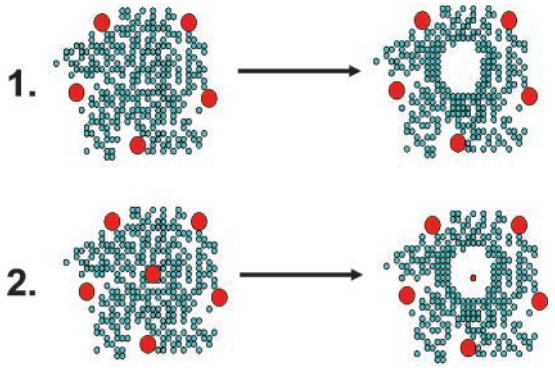

Fig. 8. Potential mechanisms of pseudopalisade formation caused by hypoxia-induced migration. One possibility is that tumor cells (*green dots*) at greatest distance from arterial supplies (*red dots*) become hypoxic after a critical point in tumor growth caused by increased metabolic demands, and migrate toward peripheral vessels, leaving a central clear zone (*1*). Alternatively, vascular occlusion or collapse within the neoplasm (illustrated as a central vessel with reduced width) could lead to central hypoxia, followed by tumor cell migration toward a viable blood supply (*2*).

late the invasive phenotype *in vitro* (28–31). *In situ* hybridization studies on human GBM specimens indicate that MMP-2 is expressed predominantly by glioma cells, whereas MMP-9 is expressed by proliferating endothelial cells (32). Therefore, we examined whether gelatinase activity was up-regulated in hypoxic glioma cells and pseudopalisades. We found that MMP-2 activity in conditioned media of glioma cells was markedly increased under hypoxia. Intense gelatinase activity also was associated with pseudopalisades using *in situ* gelatin zymography on GBM tissue sections. The combined findings provide strong evidence for gelatinase-mediated extracellular proteolytic modifications in the region of migrating hypoxic cells.

The plasminogen-activating enzyme urokinase (uPA) and its receptor, uPAR, also are up-regulated in a number of neoplasms, and increased expression correlates with invasive behavior (33–36). Hypoxia up-regulates uPAR mRNA and its cell surface protein expression in breast carcinomas (27). Our experiments did not reveal a substantial up-regulation of uPA, uPAR, or overall plasminogen activation by hypoxia *in vitro*. By immunohistochemistry, uPAR was expressed at higher levels in GBM than in surrounding normal brain but was not increased in pseudopalisades compared with adjacent astrocytoma. Neoplastic expression of uPAR and uPA may provide a permissive environment for cell migration in GBM, but their levels do not appear to be altered by hypoxia.

Although our evidence indicates that pseudopalisading cells likely represent an actively migrating population, the pathophysiologic mechanisms underlying the hypoxia-induced migration are unknown. One possibility is that cells at the greatest distance from arterial supplies become hypoxic after a critical point in tumor growth because of increased metabolic demands. Migration outward toward nearby vessels would leave a central zone that becomes necrotic (Fig. 8, mechanism 1). Another possibility is that blood vessels within the neoplasm become occluded or collapse, resulting in perivascular tumor hypoxia and cellular migration, at the site of occlusion and proximal and distal to it (Fig. 8, mechanism 2 and Fig. 9). While we cannot formally exclude the first mechanism, the latter likely accounts for a significant fraction of pseudopalisades and may be more generally relevant based on the following observations.

First, vaso-occlusion in the form of intravascular thrombosis is a well-recognized event in patients with GBMs within neoplastic tissue and at distant sites (37–39). Our studies found that 94% of GBMs had microscopic evidence of vascular thrombosis. Second, many pseudopalisades have a long, narrow, and winding (serpiginous) pattern when viewed in longitudinal tissue sections, suggesting an underlying vascular substrate associated with their emergence. Last, in some instances tumor cells form pseudopalisading structures around distorted vessels (Fig. 7*D*), degenerating vessels (Fig. 7*E*), and intravascular thrombosis (Fig. 7*F*), giving the appearance of cells migrating away.

What may initiate vascular thrombosis or occlusion? The "co-option" model of tumor progression, described recently in experimental models of metastasis and gliomas, suggests that initial tumor growth occurs around native "co-opted" blood vessels (9, 40). Once the tumor burden has reached a critical level, endothelial cells of co-opted vessels undergo angiopoietin-2-mediated apoptosis signaled through cell surface Tie-2 receptors, leading to vascular regression. If these mechanisms are relevant to human gliomas, angiopoietin-2-mediated vascular pathology could initiate pseudopalisade formation and the ensuing vascular proliferation that characterize GBM.

Opposing vaso-occlusion as a general mechanism, many pseudopalisades in tissue sections are not visibly associated with either a thrombosed vessel or a central, presumably dysfunctional vessel. Extensive necrosis within the pseudopalisade may preclude the morphologic identification of vascular structures in some cases. In addition, tissue sampling almost certainly accounts for an under-representation of vascular structures within pseudopalisades. We found that the percentage of pseudopalisades with internal vessels, thrombosis, and central necrosis increased with the width of the pseudopalisade. Tangential sectioning could lead frequently to the appearance of small pseudopalisades, which generally have fibrillar centers, lack significant necrosis, and often do not have associated vessels or thrombosis (see Fig. 7*C*, *arrow*).

In conclusion, pseudopalisades and vascular proliferation in GBM may result from the following sequence (Fig. 9): (*a*) vascular occlusion, possibly related to angiopoietin-2-mediated endothelial apoptosis, associated with intravascular thrombosis; (*b*) hypoxia in regions surrounding vascular pathology; (*c*) outward migration of glioma cells creating a migration front (pseudopalisade); (*d*) death of nonmigrated cells leading to central necrosis; (*e*) secretion of soluble proangiogenic factors (VEGF and interleukin 8) by hypoxic pseudopalisading cells; and (*f*) an exuberant angiogenic response creating "glomeruloid microvascular proliferation." Although these events represent pathologic hallmarks of GBM, it is unclear whether they are cause or conse-

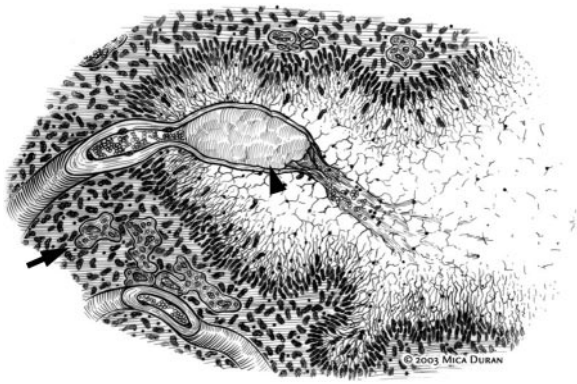

Fig. 9. Schematic representation of pseudopalisade formation in glioblastoma. Vaso-occlusion/collapse and intravascular thrombosis (*arrowhead*) lead to tissue hypoxia in the perivascular region. Hypoxic tumor cells then migrate away along cellular processes, leaving a fibrillar center initially. Hypoxia-induced cellular migration also occurs at sites proximal and distal to vaso-occlusion and thrombosis because of a lack of functional blood flow. Tumor cells that do not migrate become hypoxic and undergo apoptosis or necrosis, eventually leaving an enlarging central necrotic zone. Vessels distant to the vascular occlusion become necrotic and degenerate. Hypoxic pseudopalisading cells show increased hypoxia-inducible factor-mediated transcription and vascular endothelial growth factor secretion, leading to microvascular hyperplasia (*arrow*) nearby. Illustration by Mica Duran.

DOI:10.1158/0008-5472.CAN-03-2073

quence of increased malignancy. Given that hypoxia-induced secretion of VEGF is a major proangiogenic event and that anti-VEGF strategies reduce tumor growth, the former is more likely (7, 8, 18). Moreover, given that glomeruloid vascular proliferation is a marker of poor prognosis in other cancers (6, 10), the identification of their underlying mechanisms may have more general implications for tumor angiogenesis and malignant progression. Once identified, the pathophysiologic triggers underlying vaso-occlusion could become novel targets for antitumor therapy.

ACKNOWLEDGMENTS

We thank Holly Flinner for organizing the RTOG GBM specimens for analysis in this study.

REFERENCES

1. Kleihues, P., Burger, P. C., Collins, V. P., Newcomb, E. W., Ohgaki, H., and Cavenee, W. K. Glioblastoma. In: P. Kleihues and W. K. Cavenee, (eds). Pathology and Genetics of Tumours of the Nervous System, 2nd ed., pp. 29–39. Lyon: International Agency for Research on Cancer, 2000.
2. Brat, D. J., Castellano-Sanchez, A., Kaur, B., and Van Meir, E. G. Genetic and biologic progression in astrocytomas and their relation to angiogenic dysregulation. Adv. Anat. Pathol., *9:* 24–36, 2002.
3. Barker, F. G., 2nd, Davis, R. L., Chang, S. M., and Prados, M. D. Necrosis as a prognostic factor in glioblastoma multiforme. Cancer (Phila.), *77:* 1161–1166, 1996.
4. Burger, P. C., and Vollmer, R. T. Histologic factors of prognostic significance in the glioblastoma multiforme. Cancer (Phila.), *46:* 1179–1186, 1980.
5. Brat, D. J., Kaur, B., and Van Meir, E. G. Genetic modulation of hypoxia induced gene expression and angiogenesis: relevance to brain tumors. Front. Biosci., *8:* D100–116, 2003.
6. Brat, D. J., and Van Meir, E. G. Glomeruloid microvascular proliferation orchestrated by VPF/VEGF: a new world of angiogenesis research. Am. J. Pathol., *158:* 789–796, 2001.
7. Plate, K. H., Breier, G., Weich, H. A., and Risau, W. Vascular endothelial growth factor is a potential tumour angiogenesis factor in human gliomas *in vivo*. Nature (Lond.), *359:* 845–848, 1992.
8. Shweiki, D., Itin, A., Soffer, D., and Keshet, E. Vascular endothelial growth factor induced by hypoxia may mediate hypoxia-initiated angiogenesis. Nature (Lond.), *359:* 843–845, 1999.
9. Zagzag, D., Amirnovin, R., Greco, M. A., Yee, H., Holash, J., Wiegand, S. J., Zabski, S., Yancopoulos, G. D., and Grumet, M. Vascular apoptosis and involution in gliomas precede neovascularization: a novel concept for glioma growth and angiogenesis. Lab. Invest., *80:* 837–849, 2000.
10. Straume, O., Chappuis, P. O., Salvesen, H. B., Halvorsen, O. J., Haukaas, S. A., Goffin, J. R., Begin, L. R., Foulkes, W. D., and Akslen, L. A. Prognostic importance of glomeruloid microvascular proliferation indicates an aggressive angiogenic phenotype in human cancers. Cancer Res., *62:* 6808–6811, 2002.
11. Chan, P. T. H., and Weller, R. O. Factors influencing tumor cell and vascular proliferation in glioblastoma. Neuropathol. Appl. Neurobiol., *28:* 155–156, 2002.
12. Onda, K., Davis, R. L., Wilson, C. B., and Hoshino, T. Regional differences in bromodeoxyuridine uptake, expression of Ki-67 protein, and nucleolar organizer region counts in glioblastoma multiforme. Acta Neuropathol. (Berl)., *87:* 586–593, 1994.
13. Tachibana, O., Lampe, J., Kleihues, P., and Ohgaki, H. Preferential expression of Fas/APO1 (CD95) and apoptotic cell death in perinecrotic cells of glioblastoma multiforme. Acta Neuropathol. (Berl)., *92:* 431–434, 1996.
14. Takekawa, Y., Sawada, T., and Sakurai, I. Expression of apoptosis and its related protein in astrocytic tumors. Brain Tumor Pathol., *16:* 11–16, 1999.
15. Gown, A. M., and Willingham, M. C. Improved detection of apoptotic cells in archival paraffin sections: immunohistochemistry using antibodies to cleaved caspase 3. J. Histochem. Cytochem., *50:* 449–554, 2002.
16. Kaur, B., Brat, D. J., Calkins, C. C., and Van Meir, E. G. Brain angiogenesis inhibitor 1 is differentially expressed in normal brain and glioblastoma independently of p53 expression. Am. J. Pathol., *162:* 19–27, 2003.
17. Giannini, C., Scheithauer, B. W., Burger, P. C., Christensen, M. R., Wollan, P. C., Sebo, T. J., Forsyth, P. A., and Hayostek, C. J. Cellular proliferation in pilocytic and diffuse astrocytomas. J. Neuropathol. Exp. Neurol., *58:* 46–53, 1999.
18. Kim, K. J., Li, B., Winer, J., Armanini, M., Gillett, N., Phillips, H. S., and Ferrara, N. Inhibition of vascular endothelial growth factor-induced angiogenesis suppresses tumour growth *in vivo*. Nature (Lond.), *362:* 841–844, 1993.
19. Damert, A., Machein, M., Breier, G., Fujita, M. Q., Hanahan, D., Risau, W., and Plate, K. H. Up-regulation of vascular endothelial growth factor expression in a rat glioma is conferred by two distinct hypoxia-driven mechanisms. Cancer Res., *57:* 3860–3864, 1997.
20. Sondergaard, K. L., Hilton, D. A., Penney, M., Ollerenshaw, M., and Demaine, A. G. Expression of hypoxia-inducible factor 1α in tumours of patients with glioblastoma. Neuropathol. Appl. Neurobiol., *28:* 210–217, 2002.
21. Vordermark, D., and Brown, J. M. Evaluation of hypoxia-inducible factor-1α (HIF-1á) as an intrinsic marker of tumor hypoxia in U87 MG human glioblastoma: *in vitro* and xenograft studies. Int. J. Radiat. Oncol. Biol. Phys., *56:* 1184–1193, 2003.
22. Zagzag, D., Zhong, H., Scalzitti, J. M., Laughner, E., Simons, J. W., and Semenza, G. L. Expression of hypoxia-inducible factor 1α in brain tumors: association with angiogenesis, invasion, and progression. Cancer (Phila.), *88:* 2606–2618, 2000.
23. Krishnamachary, B., Berg-Dixon, S., Kelly, B., Agani, F., Feldser, D., Ferreira, G., Iyer, N., LaRusch, J., Pak, B., Taghavi, P., and Semenza, G. L. Regulation of colon carcinoma cell invasion by hypoxia-inducible factor 1. Cancer Res., *63:* 1138–1143, 2003.
24. Pennacchietti, S., Michieli, P., Galluzzo, M., Mazzone, M., Giordano, S., and Comoglio, P. M. Hypoxia promotes invasive growth by transcriptional activation of the met protooncogene. Cancer Cell, *3:* 347–361, 2003.
25. Zagzag, D., Nomura, M., Friedlander, D. R., Blanco, C. Y., Gagner, J. P., Nomura, N., and Newcomb, E. W. Geldanamycin inhibits migration of glioma cells *in vitro*: a potential role for hypoxia-inducible factor (HIF-1α) in glioma cell invasion. J. Cell Physiol., *196:* 394–402, 2003.
26. Ben-Yosef, Y., Lahat, N., Shapiro, S., Bitterman, H., and Miller, A. Regulation of endothelial matrix metalloproteinase-2 by hypoxia/reoxygenation. Circ. Res., *90:* 784–791, 2002.
27. Graham, C. H., Forsdike, J., Fitzgerald, C. J., and Macdonald-Goodfellow, S. Hypoxia-mediated stimulation of carcinoma cell invasiveness via upregulation of urokinase receptor expression. Int. J. Cancer, *80:* 617–623, 1999.
28. VanMeter, T. E., Rooprai, H. K., Kibble, M. M., Fillmore, H. L., Broaddus, W. C., and Pilkington, G. J. The role of matrix metalloproteinase genes in glioma invasion: co-dependent and interactive proteolysis. J. Neuro-Oncol., *53:* 213–235, 2001.
29. Yamamoto, M., Mohanam, S., Sawaya, R., Fuller, G. N., Seiki, M., Sato, H., Gokaslan, Z. L., Liotta, L. A., Nicolson, G. L., and Rao, J. S. Differential expression of membrane-type matrix metalloproteinase and its correlation with gelatinase A activation in human malignant brain tumors *in vivo* and *in vitro*. Cancer Res., *56:* 384–392, 1996.
30. Uhm, J. H., Dooley, N. P., Villemure, J. G., and Yong, V. W. Glioma invasion *in vitro*: regulation by matrix metalloprotease-2 and protein kinase C. Clin. Exp. Metastasis, *14:* 421–433, 1996.
31. Tonn, J. C., Kerkau, S., Hanke, A., Bouterfa, H., Mueller, J. G., Wagner, S., Vince, G. H., and Roosen, K. Effect of synthetic matrix-metalloproteinase inhibitors on invasive capacity and proliferation of human malignant gliomas *in vitro*. Int. J. Cancer, *80:* 764–772, 1999.
32. Raithatha, S. A., Muzik, H., Muzik, H., Rewcastle, N. B., Johnston, R. N., Edwards, D. R., and Forsyth, P. A. Localization of gelatinase-A and gelatinase-B mRNA and protein in human gliomas. Neuro-Oncol., *2:* 145–150, 2000.
33. de Vries, T. J., Quax, P. H., Denijn, M., Verrijp, K. N., Verheijen, J. H., Verspaget, H. W., Weidle, U. H., Ruiter, D. J., and van Muijen, G. N. Plasminogen activators, their inhibitors, and urokinase receptor emerge in late stages of melanocytic tumor progression. Am. J. Pathol., *144:* 70–81, 1994.
34. Blasi, F., and Carmeliet, P. uPAR: a versatile signalling orchestrator. Nat. Rev. Mol. Cell. Biol., *3:* 932–943, 2002.
35. Mori, T., Abe, T., Wakabayashi, Y., Hikawa, T., Matsuo, K., Yamada, Y., Kuwano, M., and Hori, S. Up-regulation of urokinase-type plasminogen activator and its receptor correlates with enhanced invasion activity of human glioma cells mediated by transforming growth factor-α or basic fibroblast growth factor. J. Neuro-Oncol., *46:* 115–123, 2000.
36. Mohanam, S., Sawaya, R., McCutcheon, I., Ali-Osman, F., Boyd, D., and Rao, J. S. Modulation of *in vitro* invasion of human glioblastoma cells by urokinase-type plasminogen activator receptor antibody. Cancer Res., *53:* 4143–4147, 1993.
37. Raza, S. M., Lang, F. F., Aggarwal, B. B., Fuller, G. N., Wildrick, D. M., and Sawaya, R. Necrosis and glioblastoma: a friend or a foe? A review and a hypothesis. Neurosurgery, *51:* 2–12, 2002.
38. Rodas, R. A., Fenstermaker, R. A., McKeever, P. E., Blaivas, M., Dickinson, L. D., Papadopoulos, S. M., Hoff, J. T., Hopkins, L. N., Duffy-Fronckowiak, M., and Greenberg, H. S. Correlation of intraluminal thrombosis in brain tumor vessels with postoperative thrombotic complications: a preliminary report. J. Neurosurg., *89:* 200–205, 1998.
39. Walsh, D. C., and Kakkar, A. K. Thromboembolism in brain tumors. Curr. Opin. Pulm. Med., *7:* 326–331, 2001.
40. Holash, J., Maisonpierre, P. C., Compton, D., Boland, P., Alexander, C. R., Zagzag, D., Yancopoulos, G. D., and Wiegand, S. J. Vessel cooption, regression, and growth in tumors mediated by angiopoietins and VEGF. Science (Wash. DC), *284:* 1994–1998, 1999.